International Conference on Space Optics—ICSO 2022

Dubrovnik, Croatia

3–7 October 2022

Edited by Kyriaki Minoglou, Nikos Karafolas, and Bruno Cugny,

All-semiconductor continuous-wave volumetric ranging for spaceborne differential absorption lidar

All-semiconductor continuous-wave volumetric ranging for spaceborne differential absorption lidar

Simone Bianconi[a], John A. Dykema[b], Eric A. Kittlaus[a], Mahmood Bagheri[a], and Siamak Forouhar[a]

[a]Jet Propulsion Laboratory, California Institute of Technology, Pasadena, CA, USA
[b]John A. Paulson School of Engineering and Applied Sciences, Harvard University, Cambridge, MA, USA

ABSTRACT

State-of-the-art semiconductor lasers can deliver average power, linewidth, and beam quality suitable for supporting differential absorption (DIAL) instruments that are competitive with fiber and solid-state lasers. An all-semiconductor transmitter architecture can enable a drastic reduction in size, weight, and power consumption (SWaP) of the instrument, while allowing for beneficial wavelength agility. Crucially, this reduction in SWaP can enable the implementation of compact airborne and spaceborne profiling DIAL instruments with high power output, while the broad spectral coverage of semiconductor laser technology allows the adaption and tuning of the transmitter design across a variety of operating scenarios.

In this work, we present the first demonstration of volumetric ranging based on an all-semiconductor intensity-modulated CW (IMCW) transmitter. For this proof-of-concept demonstration, we used Rayleigh backscattering in optical fiber to emulate the atmospheric backscattering return echo. The range-resolved profile is reconstructed using matched filtering of the return echo, a technique widely adopted in CW radar. Finally, we present a theoretical analysis grounded in CW radar theory, showing excellent agreement with the results measured across a wide range of transmitted waveforms and return target configurations.

Keywords: IMCW lidar, DIAL, Semiconductor laser, Planetary boundary layer

1. INTRODUCTION

Differential absorption lidar (DIAL) exploits the sounding of narrow molecular absorption lines to provide range-resolved concentration profiles of atmospheric constituents, which are crucial for the investigation of scientific planetary observables such as the terrestrial planetary boundary layer (PBL).[1]

In particular, DIAL in the near infrared (NIR) can provide crucial insight into water vapor profile and moisture structure through range-resolved sounding of water vapor. For this application, differential absorption radar (DAR) and DIAL can complement each other to deliver high-precision PBL measurements across different latitudes and cloud cover conditions. The NASA PBL Incubation Study Team report[2] determined that PBL water vapor measurements with 200 m vertical resolution, 20-25 km horizontal resolution and 10% precision are necessary to address the science questions posed in the 2018 Decadal Survey for Earth Science and Applications from Space.[1] These requirements translate to average transmitter output powers of 10-20 W, which puts particular emphasis on the wall-plug efficiency of the source, especially for airborne and spaceborne instruments, in order to limit the cost and bus complexity of the spacecraft.

The high-power pulsed solid state laser sources that are currently dominating the transmitter architecture for DIAL systems in the NIR typically exhibit wall-plug efficiencies below 1%. These systems are also typically bulky and heavy, further limiting their applicability in airborne and spaceborne instruments.[3] Furthermore, the wavelength agility and tunability of these sources is intrinsically limited by the physics of crystalline gain media and free-space optics.

---

simone.bianconi@jpl.nasa.gov

In contrast to most solid state and fiber laser sources, semiconductor lasers can be designed at any wavelength across the visible and NIR. Moreover, this class of lasers typically exhibits wall-plug efficiencies above 10%, even at Watt-level power outputs.[3–7] As a result, semiconductor lasers and power amplifiers can enable a drastic reduction in size, weight and power consumption (SWaP) of the transmitter, while allowing for highly desirable wavelength agility.

While DIAL instruments based on pulsed semiconductor transmitters have been successfully demonstrated,[8,9] the key to unlocking the full potential of semiconductor lasers lies in some form of continuous-wave (CW) range encoding scheme. This is because the peak power must be limited in order to prevent catastrophic optical damage in the semiconductor. Such CW schemes have been successfully implemented in integrated-path differential absorption (IPDA) measurements of a point target return, but have never demonstrated the volumetric ranging capabilities required for range-resolved profiling of atmospheric concentration of species such as water vapor, CO2, CH4, etc.

In this work, we leverage the matched filtering technique widely adopted in CW radar,[10] to show that CW modulation schemes can match the performance of pulsed instruments with comparable average output power. This measurement approach is analogous to chirp-modulated radar, and IMCW lidars have been demonstrated for airborne and ground-based IPDA measurements of column carbon dioxide.[3,11] Importantly, this technique is closely allied with frequency modulation continuous wave (FMCW) lidar,[12] but with two significant differences. The first difference is that the laser wavelength is held fixed, which simplifies the spectroscopic considerations necessary to perform an accurate differential absorption determination of the water vapor profile. The second difference is that IMCW is an incoherent technique, whereas FMCW is a coherent technique. The coherence aspect of FMCW can provide incredible range resolution (sub-mm and better), at the cost of stringent demands on source linewidth (¡1 kHz), beam properties (Rayleigh length must exceed 100 km), and system optical alignment (determines optical heterodyne detection efficiency).[12–14] Because sub-mm range resolution is far outside the requirements for PBL investigations, IMCW provides an attractive compromise to obtain the benefits of lightweight lidar systems with low peak power and vastly less demanding technical requirements.

In contrast to IMCW range determination in IPDA measurements of a point target return,[3,11] which has already been successfully demonstrated, range-resolved profiling of atmospheric concentration of species such as water vapor, CO2, CH4, and others, requires continuous (volumetric) ranging capability. In principle, CW volumetric ranging is achievable in lidar by retrieving the continuous reflectivity profile through Fourier analysis.[15] Here, we demonstrate volumetric ranging based on an all-semiconductor IMCW transmitter using Rayleigh backscattering in fiber to emulate the continuous atmospheric backscattering return echo. By combining spools of enhanced-Rayleigh scattering fiber[16] with several km of conventional fiber, we simulate range cells with higher atmospheric backscattering to successfully demonstrate range-resolved profile reconstruction with a resolution below 100 m. We present a detailed theoretical analysis grounded in CW radar theory which shows excellent agreement with the results measured across a wide range of transmitted waveforms and return target configurations. More importantly, this model shows that the theoretical sensitivity limit of IMCW and pulsed lidar of equal average power are equivalent.

The successful implementation of CW modulation schemes will unlock the full potential of semiconductor laser technology for inexpensive and compact spaceborne lidar instruments. The first demonstration of volumetric ranging using an all-semiconductor source presented here represents a crucial step towards the realization of space-deployable DIAL for the investigation of PBL and other applications.

2. RANGE RETRIEVAL AND MODULATION SCHEMES

We first present a theoretical analysis of CW and pulsed range retrieval schemes and compare their ideal performance. For the purpose of this discussion, we consider the return echo at a single wavelength, since the conclusions will equally apply to both the on-line and off-line DIAL wavelengths. The number of photons per acquisition in the return echo collected at the receiver of a profiling lidar instrument is related to the transmitted power by the following lidar equation:[11,17]

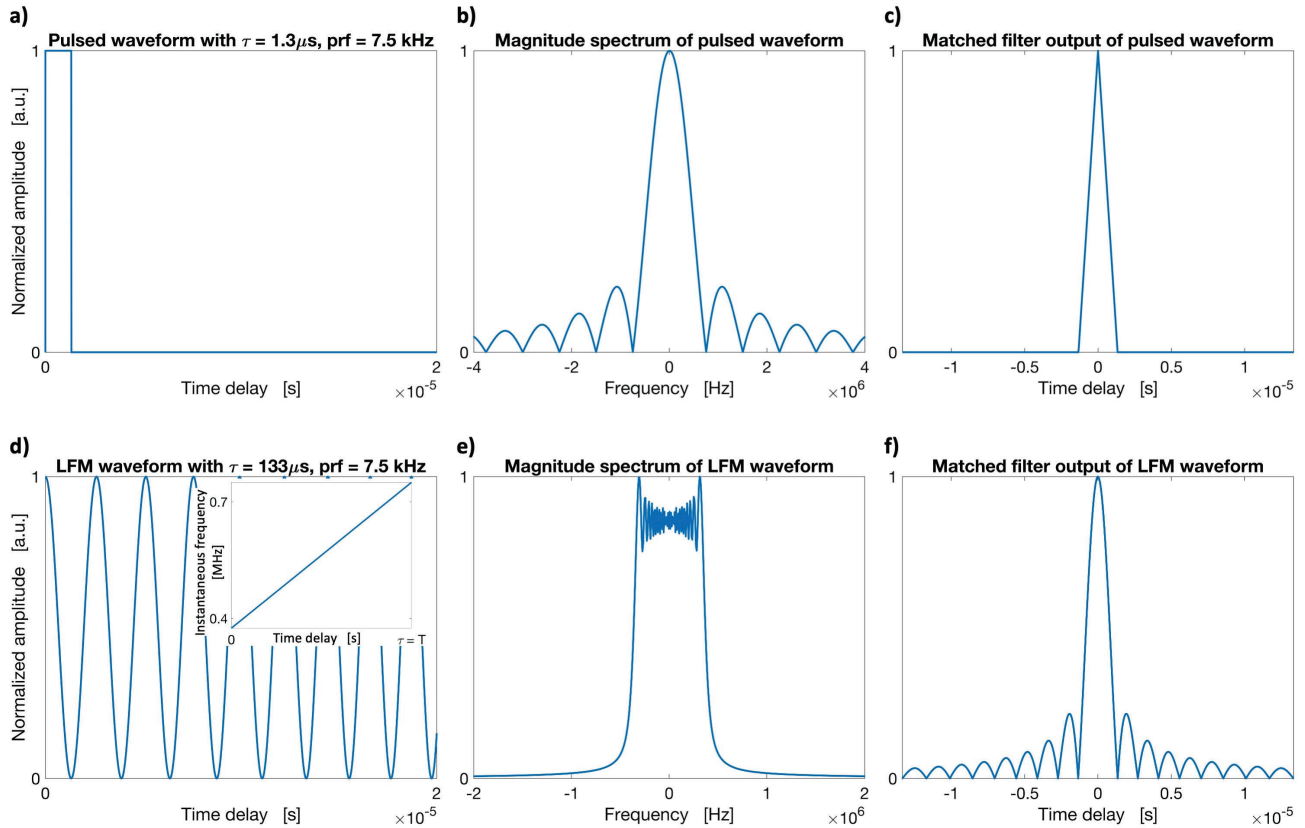$$N_S = N_L G \eta e^{-2\tau_o} \beta \Delta R \frac{A}{R_{max}^2} \qquad (1)$$

Figure 1. Pulsed and LFM waveforms and matched filter outputs. Pulsed waveform (a), spectrum (b), and matched filter output (c) for a pulse width of $\tau = 1.3 \ \mu s$ and a 7.5 kHz repetition rate. LFM waveform (d), spectrum (e), and matched filter output (f) for a 350 kHz chirp bandwidth on a 400 kHz baseline, with a 7.5 kHz repetition rate.

Here, N_L is the number of transmitted photons, G is the geometrical form (overlap) factor, η is the system optical efficiency, τ_o is the optical thickness, β the backscattering coefficient, ΔR the depth resolution, A the receiver area and R the distance from the range cell under consideration. Here, the maximum measurement range R_{max} is used in order to compute the smallest number of return photons that the receiver needs to detect. Most of these parameters are discussed in more details in the following sections. A similar lidar equation, valid for IPDA, is obtained by simply replacing the backscattering term in equation 1, i.e. the product of β and ΔR, with ρ, the surface reflectivity in sr^{-1}.[18]

2.1 Modulation schemes and matched filter

In this analysis, we consider two different modulation schemes of the transmitted waveform: pulsed and IMCW, shown in Figure 1.

The majority of state-of-the-art DIAL instruments, both ground-based and airborne, are based on a pulsed waveform with high pulse energy.[19, 20] For these systems, the depth resolution is obtained directly from the time delay of the return echo from each emitted pulse, intrinsically setting constraints on the energy, duration and repetition rate of the pulses. Conversely, in IMCW DIAL techniques the depth information is retrieved from the phase delay of the modulated waveform return echo, which allows us to relax some of the constraints on power and pulse shape, as we will show.

For the purpose of this study, we consider sources that are intrinsically pulsed by means of Q-switching or pulsed current drive, for pulsed DIAL applications. For IMCW, we assume a configuration based on a CW laser whose output is modulated at a later stage by driving an amplifier or an optical modulator (AOM or EOM) with a desired RF waveform.

For both modulation schemes we assume an ideal matched filter for the receiver frequency response and white noise. This signal processing technique guarantees the maximum achievable SNR for any given transmitted waveform,[10] and hence enables a fair comparison between the two modulation schemes under consideration. It is worth noting, however, that the vast majority of pulsed lidar receivers employ a simple lowpass or bandpass filter frequency response, which can only achieve 82% of the matched filter SNR.[21] The matched filter frequency response for a transmitted waveform spectrum $X(\Omega)$ is given by:[10]

$$H(\Omega) = \alpha X^*(\Omega) e^{-j\Omega T_M} \tag{2}$$

with α an arbitrary gain constant and T_M an arbitrary time delay. The waveform spectra and resulting matched filter outputs for both pulsed and a linear frequency-modulated (LFM) IMCW modulation schemes are shown in Figure 1.

In a pulsed DIAL system the vertical resolution is determined by the pulse duration, τ, as shown by the width of the matched filter output in Figure 1c:[10]

$$\Delta R = \frac{c\tau}{2} \tag{3}$$

Conversely, for an LFM waveform the resolution is represented by the peak-to-first null distance in the matched filter output in Figure 1f, and is related to the chirp bandwidth β and independent of the pulse duration:[10]

$$\Delta R = \frac{c}{2\beta} \tag{4}$$

As a result, the IMCW modulation scheme enables de-coupling of the pulse duration and range resolution.[10] The pulse duration is therefore no longer fixed by the resolution but only bounded by the pulse repetition period, i.e. $\tau < T$.

The maximum pulse repetition frequency ($f_{pr} = 1/T$) is limited by the unambiguous range R_{ua}, which should be larger than the maximum measurement range R_{max} (unless specialized range disambiguation techniques are used):[10]

$$R_{ua} = \frac{cT}{2} \geq R_{max} \tag{5}$$

2.2 SNR analysis

The maximum achievable SNR versus white noise for any given transmitted waveform is achieved with matched filtering, and given by:[10]

$$SNR = \frac{E}{\sigma_w^2} \tag{6}$$

with E the total energy in the signal $x(t)$, and σ_w^2 the noise spectral density, both in W/Hz. Remarkably, the use of matched filtering implies that the maximum achievable SNR depends only on the energy of the signal waveform and not on other details such as the modulation scheme. The total spectral energy of the waveform in W/Hz is expressed by:[10]

$$E = R_0 \int_0^T |x(t)|^2 dt \tag{7}$$

where R_0 is the readout resistance, and $x(t)$ represents the detector photocurrent from the return echo. Considering the case of shot noise-limited performance, the noise spectral density can be expressed as $\sigma_w^2 = R_0 \langle I_n^2 \rangle = 2qgR_0\langle x(t) \rangle$ in W/Hz, with q the fundamental charge and g the internal gain of the photodetector.[22]
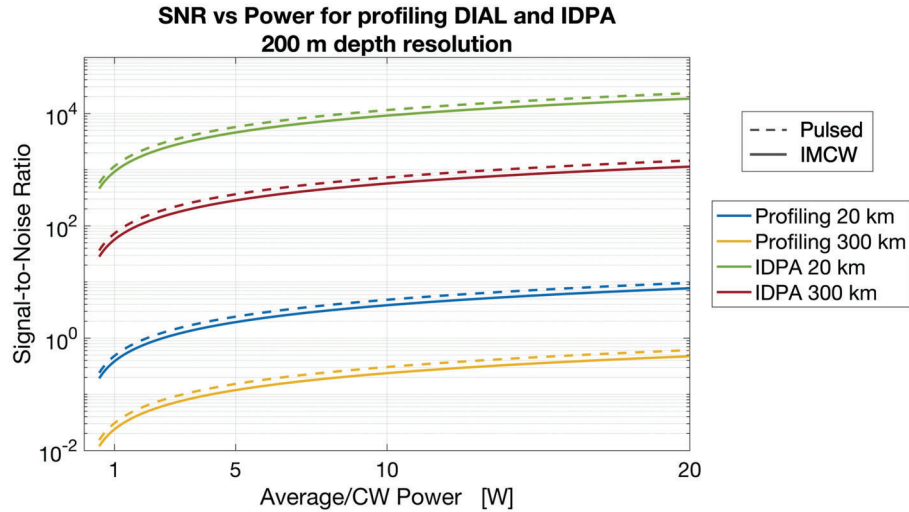
Figure 2. SNR as a function of transmitter average power for both pulsed (dashed line) and IMCW (solid line) lidar. For all four the simulated scenarios, including both profiling DIAL and IPDA, the SNR of IMCW is compared to that of pulsed instruments.

The matched filter SNR can then be expressed as a function of the number of photons in the return echo for both pulsed and IMCW lidar systems, as:

$$SNR = \alpha \eta N_{ph} \tag{8}$$

where N_{ph} is the total number of photons in the return echo waveform and η is the quantum efficiency of the detector. Here, α is a factor arising from the integral in equation 7, which depends on the modulation scheme. For pulsed lidar systems, the source average power and the pulse repetition frequency yield the total energy of a pulse, which is equal to the pulse amplitude multiplied by the pulse duration $E = P_{ave}/f_{pr} = P_{peak}\tau$, yielding $\alpha = 0.5$. For IMCW systems, assuming a 100% depth of modulation, the average power is half of the CW power and the energy of a pulse is $E = P_{CW}/2f_{pr}$, yielding $\alpha = 0.75$. The number of photons in the return echo is related to the transmitted power by equation 1, allowing the estimation of the instrument SNR as a function of source laser power output in different scenarios, as shown in Figure 2.

Figure 2 offers a comparison between the SNR achieved with pulsed and IMCW modulation schemes in a few typical scenarios, such as profiling DIAL and IPDA, at 20 and 300 km range. IMCW enables SNR values that are virtually identical (within a few %) to those of pulsed systems, for the same average transmitted power. Notably, in pulsed systems the transmitted power is concentrated in a short pulse, resulting in kilowatt-level peak powers. Conversely, in IMCW the pulse width is no longer limited by the depth resolution, which allows the extension of the duration of the pulse up to the repetition period upper bound (i.e. $\tau = T$). This in turn translates into much lower peak power, which can be supplied, for example, by watt-class CW semiconductor lasers.

3. IMCW VOLUMETRIC RANGING

In order to demonstrate volumetric ranging using a CW modulation scheme in the laboratory, we leverage Rayleigh backscattering in optical fiber to emulate the continuous atmospheric backscattering return echo. Figure 3 shows a schematic of setup employed for the experimental demonstration that we performed in the lab compared to that of a conventional DIAL instrument for atmospheric profiling.

The transmitter architecture is extremely similar, and the transmitter/receiver optics and atmosphere are emulated in the laboratory using a circulator and spools of optical fiber. In particular, we employed two different types of fiber at 1550 nm: a 10 km spool of a conventional optical fiber (Corning SMF-28) as well as 270 m
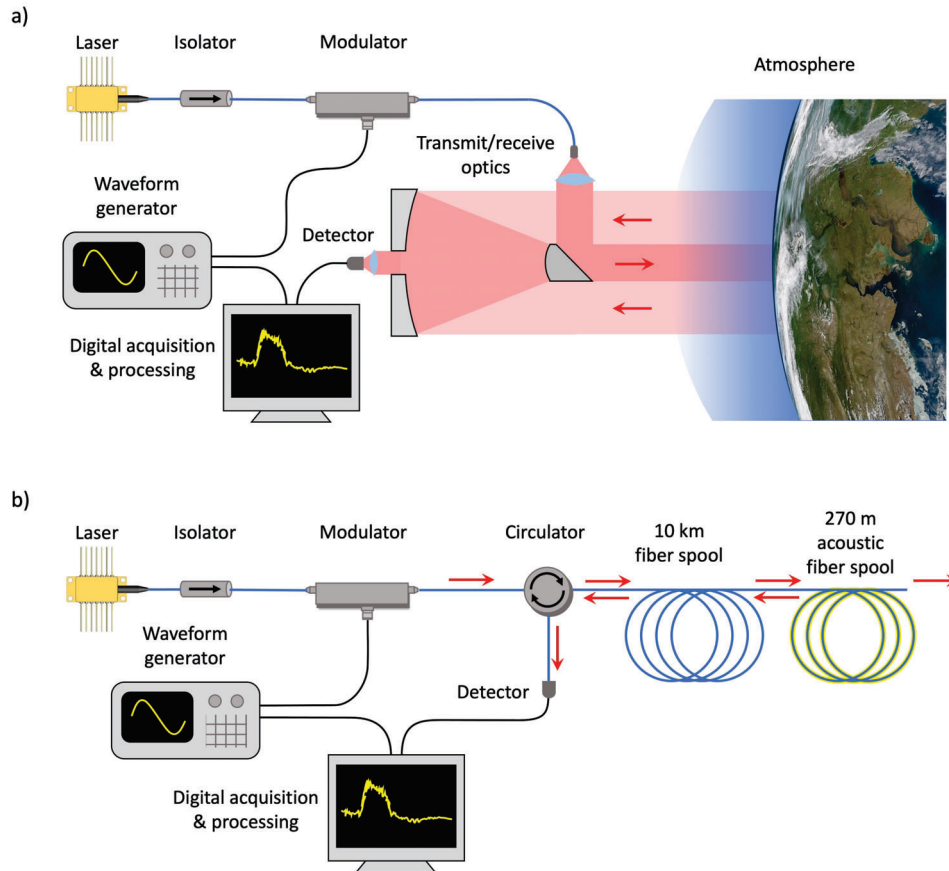
Figure 3. Instrument schematic of an IMCW DIAL for atmospheric profiling (a) and corresponding experimental setup employing Rayleigh backscattering in fiber spools to simulate continuous atmospheric backscattering (b). The acoustic fiber spools with enhanced backscattering highlighted in yellow were only included in some of the experiments.

of a fiber designed for distributed acoustic sensing with enhanced Rayleigh backscattering (OFS Acoustisens). The latter is useful for simulating common scenarios in PBL profiling, where a few range cells have significantly higher backscattering.

Since volumetric ranging using pulsed transmitted waveforms is well understood,[8,9] we replicated all following measurements both using pulsed and IMCW schemes, in order to compare their performance. For IMCW ranging we utilized a narrow-linewidth laser center at 1550 nm emission wavelength (TeraXion NLL) and an amplitude modulator (JDS Uniphase) combined with a polarization controller, to modulate the transmitted signal. For pulsed ranging, we pulsed the laser (Thorlabs FPL1007S) directly using a pulse current generator (ILX Lightwave LDP-3811), while maintaining the modulator and polarization controller in the setup in order to minimize changes in the experimental parameters. The photodetector employed is a fiber-coupled InGaAs photodiode (Koheron PD100-DC), and the time-resolved return signal is saved using a 40 Gbps oscilloscope (LeCroy WavePro) and matched filtering is performed off-line using Matlab scripts we developed. The return power is measures using a pick-off at a 99-1 splitter: the backscattering return from a 10 km spool of SMF-28 fiber is -56 dB.

Figure 4 shows volumetric ranging results for several different experimental conditions. Here, we report both volumetric ranging of uniform backscattering profile from a 10 km spool of SMF-28 fiber (Figure 4 a, b, c), as well as a 10 km spool of SMF-28 fiber followed by 270 m of enhanced backscattering fiber, to simulated a PBL profiling scenario (Figure 4 d, e, f). The range determination precision is comparable for pulsed and IMCW measurements, while the peak power of the pulsed measurements is around 100 times higher than the CW power of the IMCW ones.
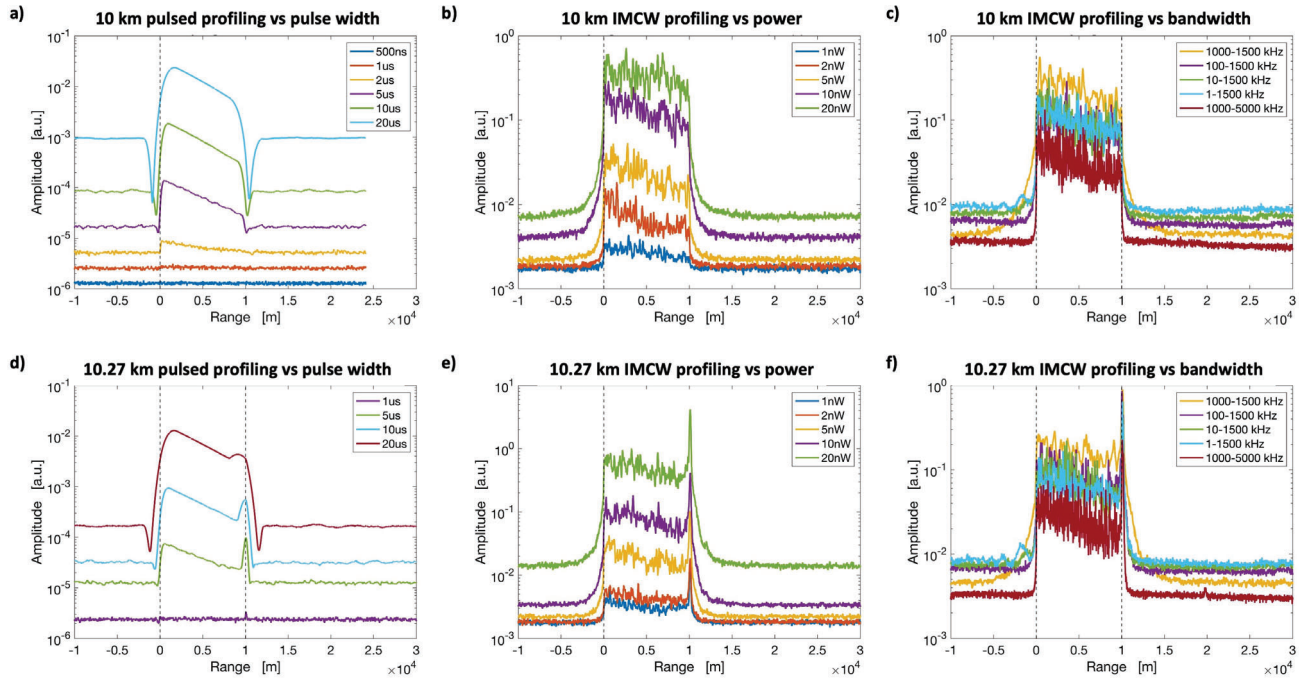
Figure 4. Volumetric ranging measurements for both pulsed and IMCW for a variety of experimental conditions. The top three panels (a,b, c) are for a 10 km spool of SMF28 fiber, while the bottom three panels (d, e, f) for the same 10 km spool followed by 270 m spools of acoustic fiber with enhanced backscattering. Panels a) and c) correspond to different pulse widths, b) and e) to different measured average power, and c) and f) to different sweep bandwidths. Since the peak power of the pulsed waveform in panels a) and c) is kept constant, the varying pulse width also corresponds to varying average power.

Figure 4 a, c show pulsed volumetric ranging as a function of pulse width. As discussed in the previous sections, the pulse width determines the range resolution in a pulsed measurement. In these measurements, the peak power was kept constant, and as a result changes in the pulse width result in proportional changes in average transmitted power.

Figure 4 b, e show IMCW volumetric ranging as a function of average transmitted power. The power reported in the legend is the average return echo power measured at the detector.

As discussed in the previous sections, in IMCW ranging the range resolution is independent of the transmitted power, and is instead determined solely by the bandwidth of the waveform. Figure 4 c, f show IMCW volumetric ranging as a function of waveform bandwidth: as the bandwidth increases, the boundaries of the scattering profiles as well as the enhanced backscattering cells are resolved more sharply, at the cost of diminished SNR.

3.1 Volumetric ranging numerical model

The experimental volumetric ranging results were modeled numerically using the theory detailed in the previous sections. In particular, we used Monte Carlo simulations to generate a noisy pattern on the return echo based on the shot noise contributions of both dark and photo-current, expressed as:[22]

$$I_n = \sqrt{2qIBW} \tag{9}$$

where I is either the dark or the photo-current and BW is the detector bandwidth. The simulated noisy returns were then averaged in the same manner as for the ranging measurements. Besides pulsed and IMCW ranging, we also included a range determination scheme based on pseudo-random binary sequence (PRBS) encoding, which has been employed in some DIAL instruments,[3, 23] in order to compare their performances.
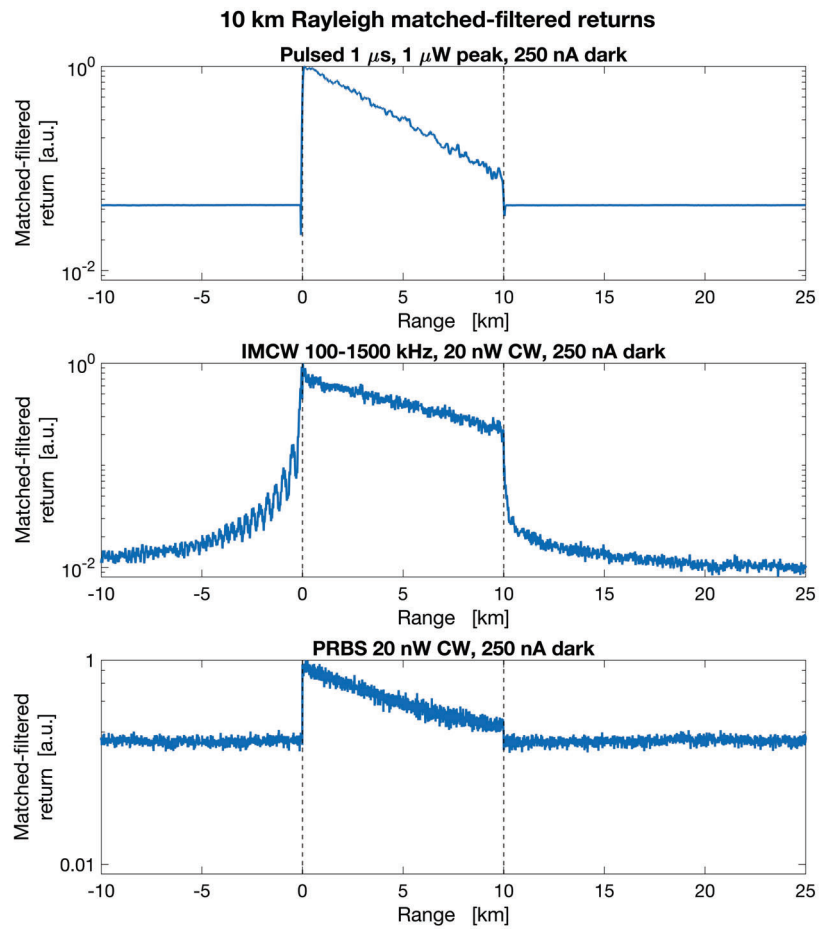
Figure 5. Modeled volumetric ranging of a uniform 10 km backscattering target for pulsed (top), IMCW (middle) and PRBS (bottom) range encoding schemes. The modeled ranging conditions (pulse duration, peak and CW power, chirp bandwidth etc.) are specified in the titles of each panel.
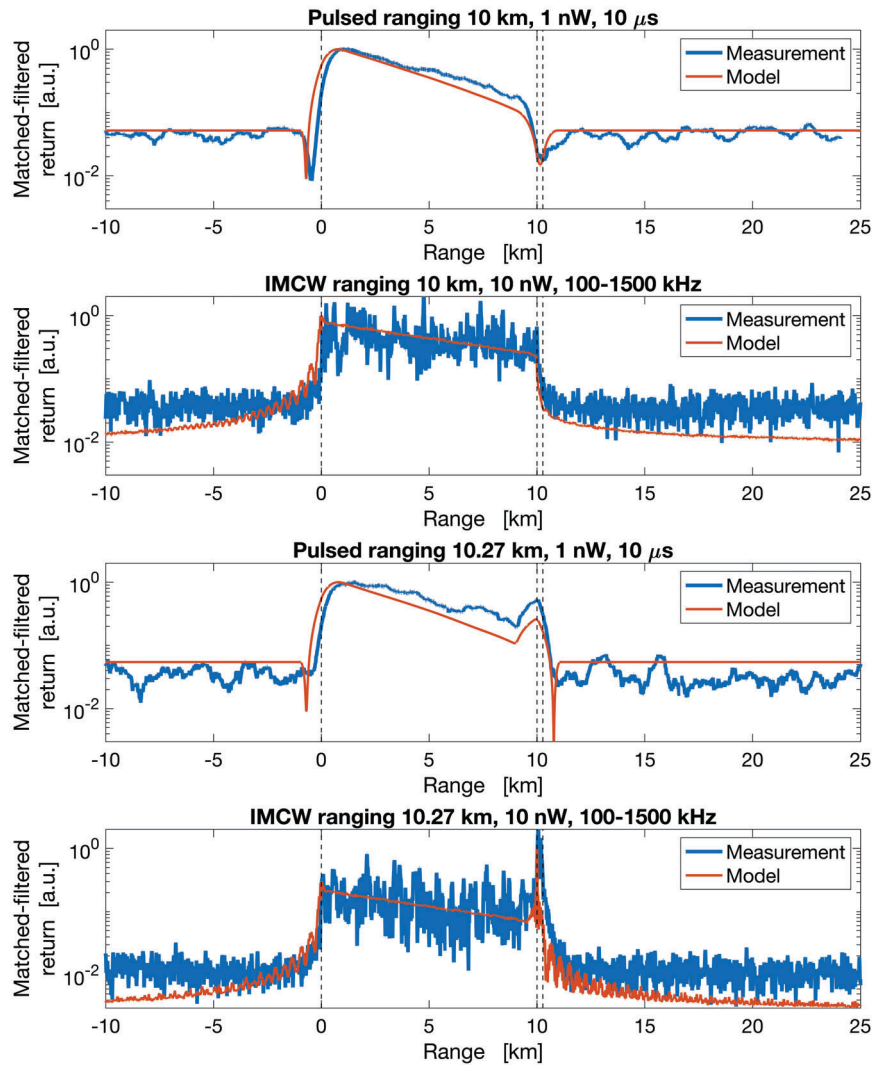
Figure 6. Measured and modeled volumetric ranging for both pulsed and IMCW. The top two panels are for a 10 km spool of SMF28 fiber, while the bottom two panels for the same 10 km spool followed by 270 m spools of acoustic fiber with enhanced backscattering. The modeled ranging conditions (pulse duration, measured average power, chirp bandwidth etc.) are specified in the titles of each panel.
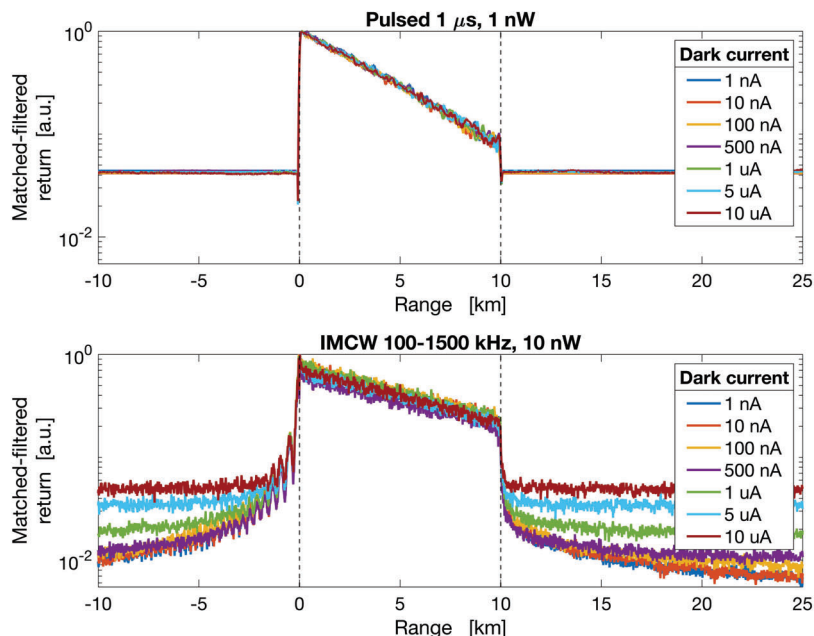
Figure 7. Modeled volumetric ranging of a uniform 10 km scattering target for both pulsed (top) and IMCW (bottom) as a function of detector dark current. The modeled ranging conditions (pulse duration, peak and CW power, chirp bandwidth etc.) are specified in the titles of each panel.

Figure 5 shows the matched-filtered return echo from a 10 km volumetric target for the three range retrieval schemes at standard experimental conditions (250 nA detector dark current, 10 km spool of SMF28), for comparable average transmitted power. The IMCW profiling measurements exhibits the highest SNR of the three, followed by the pulsed measurements, due to improved spectral filtering of the photon shot noise, as discussed above.[10, 21]

Figure 6 shows a comparison between the measurements and the numerical model for four different experimental conditions, including both a uniform backscattering profile (10 km spool of SMF28 fiber) and an enhanced backscattering profile (10 km spool of SMF28 fiber followed by 270 m of acoustic fiber). Here, both measurements and simulations were averaged over 1000 acquisitions. The model shows excellent agreement with the measurements for both pulsed and IMCW ranging. The power reported for these measurements is the average power measured at the detector: while the average power is lower for the pulsed measurements, the peak power in such measurements is 50 times higher than the CW power.

The numerical model enabled us to investigate additional measurement conditions, such as different detector dark currents, and different backscattering profiles. Because of the nature of matched filtering, an IMCW ranging measurement entails spectral filtering of the return echo, which can prove advantageous in many scenarios, but requires careful considerations on the experimental conditions for optimal precision. As an example, a perfectly flat return profile spanning the entirety of the unambiguous range is extremely challenging to range with a non-zero base-band IMCW waveform. Fortunately, the discontinuous nature of photon shot noise and backscattering generates a discontinuous return echo which can be effectively discriminated with IMCW profiling. This discontinuous return echo is then averaged over time to produce a smooth profile almost analogous to that obtained for pulsed ranging. In addition, pulsed ranging schemes are more effective than IMCW at filtering dark noise, thanks to extremely low pulse duty cycles, as show in Figure 7. Here, we artificially varied the detector dark current while maintaining other measurements parameters fixed, and showed that the SNR of IMCW volumetric ranging is significantly affected by dark current, unlike that of pulsed ranging.

4. CONCLUSION

In this work, we demonstrated that all-semiconductor high-power CW laser sources constitute a viable alternative to the current state-of-the-art pulsed systems for supporting a new class of compact and efficient spaceborne DIAL instruments. We showed that the optimal DIAL performance (achieved using matched filtering) of CW laser sources in an IMCW modulation scheme closely matches that of a pulsed system for a similar average laser power output. We demonstrated volumetric ranging based on an all-semiconductor IMCW transmitter using Rayleigh backscattering in fiber to emulate the atmospheric backscattering return echo. Finally, we implemented a detailed model of the range determination schemes showing excellent agreement with the results measured across a wide range of transmitted waveforms and return target configurations, and we presented insights into optimal waveform choice for IMCW volumetric ranging for differing target configurations.

ACKNOWLEDGMENTS

REFERENCES

[1] Space Studies Board, National Academies of Sciences, Engineering, and Medicine and others, [*Thriving on our changing planet: A decadal strategy for Earth observation from space*], National Academies Press (2019).

[2] Teixeira, J., Piepmeier, J., and Nehrir, A., "Nasa incubation study on planetary boundary layer," in [*IGARSS 2020-2020 IEEE International Geoscience and Remote Sensing Symposium*], 6144–6145, IEEE (2020).

[3] Ai, X., Pérez-Serrano, A., Quatrevalet, M., Nock, R. W., Dahnoun, N., Ehret, G., Esquivias, I., and Rarity, J. G., "Analysis of a random modulation single photon counting differential absorption lidar system for space-borne atmospheric co 2 sensing," *Optics express* **24**(18), 21119–21133 (2016).

[4] Schwertfeger, S., Wiedmann, J., Sumpf, B., Klehr, A., Dittmar, F., Knauer, A., Erbert, G., and Trankle, G., "7.4 w continuous-wave output power of master oscillator power amplifier system at 1083 nm," *Electronics Letters* **42**(6), 346–347 (2006).

[5] Fiebig, C., Blume, G., Kaspari, C., Feise, D., Fricke, J., Matalla, M., John, W., Wenzel, H., Paschke, K., and Erbert, G., "12 w high-brightness single-frequency dbr tapered diode laser," *Electronics letters* **44**(21), 1253–1255 (2008).

[6] Chi, M., Jensen, O. B., Holm, J., Pedersen, C., Andersen, P. E., Erbert, G., Sumpf, B., and Petersen, P. M., "Tunable high-power narrow-linewidth semiconductor laser based on an external-cavity tapered amplifier," *Optics express* **13**(26), 10589–10596 (2005).

[7] Chi, M., Müller, A., Hansen, A. K., Jensen, O. B., Petersen, P. M., and Sumpf, B., "Micro-integrated high-power narrow-linewidth external-cavity tapered diode laser at 808 nm," *Applied optics* **59**(2), 295–299 (2020).

[8] Nehrir, A. R., Repasky, K. S., and Carlsten, J. L., "Micropulse water vapor differential absorption lidar: transmitter design and performance," *Optics express* **20**(22), 25137–25151 (2012).

[9] Spuler, S. M., Hayman, M., Stillwell, R. A., Carnes, J., Bernatsky, T., and Repasky, K. S., "Micropulse dial (mpd)–a diode-laser-based lidar architecture for quantitative atmospheric profiling," *Atmospheric Measurement Techniques* **14**(6), 4593–4616 (2021).

[10] Richards, M. A., [*Fundamentals of radar signal processing*], McGraw-Hill Education (2014).

[11] Dobler, J. T., Harrison, F. W., Browell, E. V., Lin, B., McGregor, D., Kooi, S., Choi, Y., and Ismail, S., "Atmospheric co 2 column measurements with an airborne intensity-modulated continuous wave 1.57 μm fiber laser lidar," *Applied optics* **52**(12), 2874–2892 (2013).

[12] Dieckmann, A., "Fmcw-lidar with tunable twin-guide laser diode," *Electronics Letters* **30**(4), 308–309 (1994).

[13] Martin, A., Dodane, D., Leviandier, L., Dolfi, D., Naughton, A., O'Brien, P., Spuessens, T., Baets, R., Lepage, G., Verheyen, P., et al., "Photonic integrated circuit-based fmcw coherent lidar," *Journal of Lightwave Technology* **36**(19), 4640–4645 (2018).

[14] Isaac, B. J., Song, B., Pinna, S., Coldren, L. A., and Klamkin, J., "Indium phosphide photonic integrated circuit transceiver for fmcw lidar," *IEEE Journal of Selected Topics in Quantum Electronics* **25**(6), 1–7 (2019).

[15] Barber, Z. W., Dahl, J. R., Sharpe, T. L., and Erkmen, B. I., "Shot noise statistics and information theory of sensitivity limits in frequency-modulated continuous-wave ladar," *JOSA A* **30**(7), 1335–1341 (2013).

[16] Hart, J. D., Hutchinson, M. N., and Cranch, G. A., "Comparison of all-grating fiber and enhanced backscatter fiber for distributed strain sensing," in [*Optical Fiber Sensors*], T1–5, Optica Publishing Group (2020).

[17] Weitkamp, C., [*Lidar: range-resolved optical remote sensing of the atmosphere*], vol. 102, Springer Science & Business (2006).

[18] Ehret, G., Kiemle, C., Wirth, M., Amediek, A., Fix, A., and Houweling, S., "Space-borne remote sensing of co 2, ch 4, and n 2 o by integrated path differential absorption lidar: a sensitivity analysis," *Applied Physics B* **90**(3), 593–608 (2008).

[19] Wulfmeyer, V. and Walther, C., "Future performance of ground-based and airborne water-vapor differential absorption lidar. i. overview and theory," *Applied Optics* **40**(30), 5304–5320 (2001).

[20] Nehrir, A. R., Hair, J. W., Ferrare, R. A., Hostetler, C. A., Kooi, S. A., Notari, A., Harper, D. B., Collins Jr, J., Barton-Grimley, R. A., Antill, C., et al., "The high altitude lidar observatory (halo): A multi-function lidar and technology testbed for airborne and space-based measurements of water vapor and methane," in [*AGU Fall Meeting Abstracts*], **2018**, A31P–3155 (2018).

[21] North, D. O., "An analysis of the factors which determine signal/noise discrimination in pulsed-carrier systems," *Proceedings of the IEEE* **51**(7), 1016–1027 (1963).

[22] Bianconi, S. and Mohseni, H., "Recent advances in infrared imagers: toward thermodynamic and quantum limits of photon sensitivity," *Reports on Progress in Physics* **83**(4), 044101 (2020).

[23] Quatrevalet, M., Ai, X., Pérez-Serrano, A., Adamiec, P., Barbero, J., Fix, A., Tijero, J. M. G., Esquivias, I., Rarity, J. G., and Ehret, G., "Atmospheric co $_2$ sensing with a random modulation continuous wave integrated path differential absorption lidar," *IEEE Journal of Selected Topics in Quantum Electronics* **23**(2), 157–167 (2016).